JOURNAL OF APPLIED ELECTROCHEMISTRY 20 (1990) 575–585

A general computational method for mass-transport problems involving wall–jet electrodes and its application to simple electron-transfer, ECE and DISP1 reactions

R. G. COMPTON, C. R. GREAVES, A. M. WALLER

Physical Chemistry Laboratory, Oxford University, South Parks Road, Oxford OX1 3QZ

Received 15 August 1989; finally revised 2 October 1989

A computational procedure based on the Backwards Implicit Method is shown to be a powerful and general method of solving problems of mass transport to a wall–jet electrode. Conventional numerical methods based on a Cartesian grid are unsatisfactory because the electrode is very non-uniformly accessible. An expanding grid which increases in size in proportion to the diffusion layer thickness across the electrode surface, is shown to be effective in computing the limiting current–flow rate behaviour of (a) a simple electron-transfer reaction, (b) ECE, and (c) DISP1 processes.

1. Introduction

The wall–jet electrode (WJE) is a well-characterised and increasingly popular hydrodynamic electrode in which the flow is due to a fluid jet which strikes a planar electrode surface at right-angles and spreads out radially over that surface; the fluid outside the jet being at rest [1]. This pattern of flow is sketched schematically in Fig. 1. The WJE has been enthusiastically adopted by electroanalytical chemists partly because as a flow cell it is well suited to continuous monitoring analysis. In particular it has been developed for use with such techniques as anodic stripping voltammetry [2–4], flow-injection analysis [5–7] and HPLC detection [8, 9]; in all of which its sensitivity, well-defined hydrodynamics, robust shape and ease of practical use have been considered advantageous [10]. A double WJE has been described [11, 12] and again used hitherto exclusively for analytical work [13].

We are unaware of any applications of the wall–jet in the study of electrode reaction mechanisms although the fact that it is very-non-uniformly accessible (see below) might lead one to anticipate that it might be particularly powerful in terms of mechanistic discrimination [14, 15]. Part of this neglect arises from the absence of any generally applicable theory of mass transport to such electrodes; in particular for electrode processes involving coupled homogeneous kinetics. Previous treatments – restricted to simple, kinetically uncomplicated electron-transfer reactions – have relied on analytical methods of solving the appropriate convective-diffusion equations [11, 16] and this approach may not be readily applicable to more complex and interesting electrode processes. Accordingly we present, in this paper, a general computational strategy for solving mass-transport problems at WJEs. The method is shown first to give results in good agreement with the existing analytical solutions for simple electron-transfer and is then extended to the cases of the ECE and the DISP1 reaction mechanisms. Before presenting the new theory we briefly review the hydrodynamics of the wall–jet arrangement.

2. The hydrodynamics of the WJE

The theory of fluid motion for the WJE under laminar flow conditions was derived by Glauert [1]. Using the coordinates defined in Fig. 1, the velocity of the solution is described by two components: v_r for the radial velocity, and v_z for the velocity in the direction normal to the electrode surface. It is convenient to define a dimensionless parameter η, where η describes distance normal to the 'wall' and is given by

$$\eta = (135M/32v^3r^5)^{1/4}z \quad (1)$$

where v is the kinematic viscosity and $M = k_c^4 V_f^3/2\pi^3 a^2$ in which V_f is the volume flow rate ($cm^3 s^{-1}$), k_c is a constant determined by experiment (see below) and a is the diameter of the jet. v_r is given by

$$v_r = (15M/2vr^3)^{1/2} f'(\eta) \quad (2)$$

and v_z by

$$v_z = (3/4)\,(40Mv/3r^5)^{1/4} h(\eta) \quad (3)$$

The functions $f'(\eta)$ and $h(\eta)$ are shown in Fig. 2 and may be generated from the following functions:

$$f'(\eta) = (2g/3)\,(1 - g^3) \quad (4)$$

$$f(\eta) = g^2 \quad (5)$$

$$\eta = \ln[(1 + g + g^2)^{1/2}/(1 - g)] + 3^{1/2} \arctan\,[3^{1/2}g/(2 + g)] \quad (6)$$

$$h(\eta) = (5/3)\eta f'(\eta) - f(\eta) \quad (7)$$

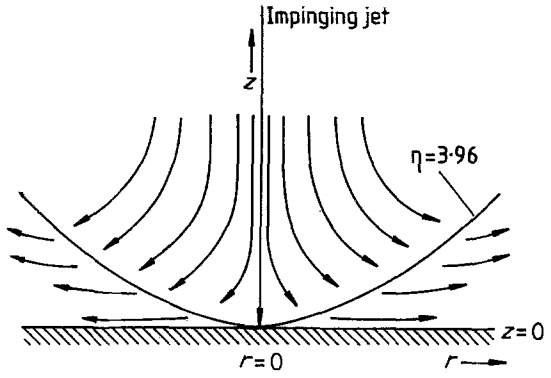

Fig. 1. The flow pattern at the wall-jet electrode.

by varying g from 0 to 1 so that η varies from 0 to infinity. From Fig. 2 it can be seen that both v_r and v_z decrease as r increases. v_r is zero at the wall, passes through a maximum at $\eta = 2.03$ and then declines back to zero, whereas v_z, again zero at the wall, reaches a maximum value at $\eta = 2.31$ and drops back to zero at $\eta = 3.96$. For all these values of η, the flow is away from the wall. For values of η larger than 3.96, $h(\eta)$ is negative, reaching a limiting value of -1 far from the wall. Flow in this region is thus towards the wall. That is, there exists a boundary at $\eta = 3.96$ dividing flow towards the electrode from that moving away. This boundary and schematic streamlines are shown in Fig. 1. It can be seen from this figure that the WJE is a highly non-uniformly-accessible electrode – that rates of mass transport are much greater in the centre of the electrode than at the edges. This is shown quantitatively by the fact that the diffusion layer thickness, δ_d, at a WJE is proportional to $r^{5/4}$ [11] (see below).

3. Simple electron transfer at a WJE

The form of the convective-diffusion equation relevant to the WJE geometry, under steady-state conditions is

$$v_r \frac{\partial c}{\partial r} + v_z \frac{\partial c}{\partial z} = D \frac{\partial^2 c}{\partial z^2} \tag{8}$$

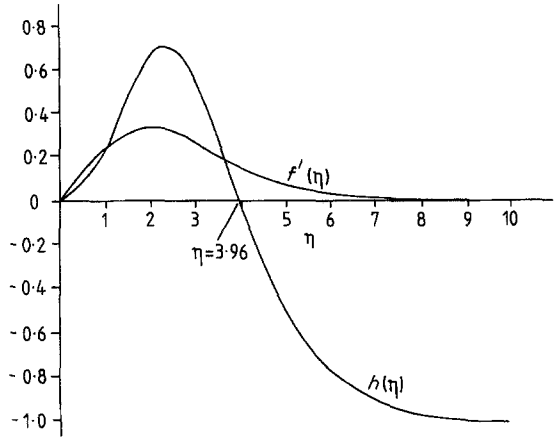

Fig. 2. The velocity profiles for the radial velocity, $f'(\eta)$, and the normal velocity, $h(\eta)$, as a function of the dimensionless coordinate, η.

where c is the concentration of the species of interest, D its diffusion coefficient and v_r and v_z have been defined above. In writing Equation 8 we have neglected radial diffusion, which has been shown to be a good approximation for practical electrodes [11]. To solve the above equation we need to specify appropriate boundary conditions. For the case of a simple electron-transfer reaction

$$A + e^- \longrightarrow B \tag{I}$$

under transport-limited conditions these take the form

$$\text{(a) } z = 0, \quad [A] = 0$$

$$\text{(b) } z \longrightarrow \infty, \quad [A] \longrightarrow [A]_0$$

where $[A]_0$ represents the concentration of A in bulk solution.

In order to solve Equation 8 we approximate the derivatives to their finite-difference equivalents. The r–z plane is thus divided up into a two-dimensional grid as shown in Fig. 3. Increments in the r direction are Δr and in the z direction Δz. We use the subscripts k and j to denote distances on the radial and normal directions

$$\text{(radial distance)}_k = k\Delta r,$$

$$k = 0, 1, \ldots, K \quad \text{where } \Delta r = R/K \tag{9}$$

$$\text{(normal distance)}_j = j\Delta z,$$

$$j = 0, 1, \ldots, J \quad \text{where } \Delta z = Z/J \tag{10}$$

where R is the radius of the electrode and Z is the length of the grid in the z direction.

The derivatives in Equation 8 become

$$\left.\frac{\partial g}{\partial r}\right|_{j,k+1} = \frac{g_{j,k+1} - g_{j,k}}{\Delta r} \tag{11}$$

$$\left.\frac{\partial g}{\partial z}\right|_{j,k+1} = \frac{g_{j+1,k+1} - g_{j,k+1}}{\Delta z} \tag{12}$$

$$\left.\frac{\partial^2 g}{\partial z^2}\right| = \frac{g_{j+1,k+1} - 2g_{j,k+1} + g_{j-1,k+1}}{(\Delta z)^2} \tag{13}$$

where g is the normalised concentration of A, i.e.

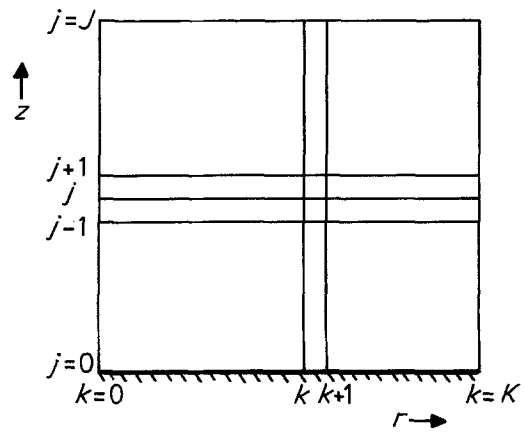

Fig. 3. The finite-difference grid.

$g = [A]/[A]_0$. The boundary conditions are

$$j = 0, \quad g_{0,k} = 0 \quad 1 < k < K \tag{14}$$

$$k = 0, \quad g_{j,0} = 1 \quad 1 < j < J \tag{15}$$

$$j = J, \quad g_{J,k} = 1 \quad 0 < k < K \tag{16}$$

The above approach combined with the Backwards Implicit Method has been successfully applied to a great diversity of problems in the field of channel electrodes [17–24]. However the WJE displays a much greater non-uniformity of accessibility than the channel electrode [25]. Thus if a simple Cartesian grid were adopted, as in Fig. 3, unsatisfactory results would be likely. This is because, as can be seen from Fig. 1, the diffusion layer thickness varies as $r^{5/4}$. Thus if an appropriate value of Δr is chosen so that a sufficient number of grid points is used at small values of r to cover the diffusion layer thickness and thus ensure convergence, the total number of grid points used in the calculation will be prohibitively large since the same value of Δr will apply at the outside of the electrode where the diffusion layer is very much thicker. Moreover such a calculation would be extremely inefficient as, for small r, the vast majority of the grid points would lie outside of the diffusion layer and thus be inconsequential to the computation because $g_{j,k}$ would be unity for these points.

To overcome these difficulties we develop an expanding grid approach where the size of Z increases with k. For every value of r ($= k\Delta r$) we restrict the grid to within a selected range of η from 0 to η^*, so that all the concentration changes occur within this region. As will be discussed below, a value of 0.4 for η^* is found to be optimal. The corresponding value of Z is given by

$$Z = \eta^*[135M/(32v^3(k\Delta r)^5)]^{-1/4} \tag{17}$$

A schematic diagram of the expanding grid is shown in Fig. 4. We use the notation z_k to denote the line normal to the electrode surface, between $z = 0$ and $z = Z_k$, in this figure.

In the Backwards Implicit Method [17] the normalised concentrations of A along z_{k+1} are calculated from those along z_k. In order to do this, a Cartesian

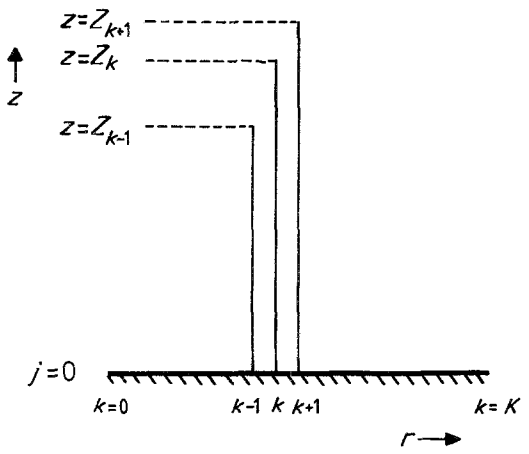

Fig. 4. A schematic representation of the expanding grid.

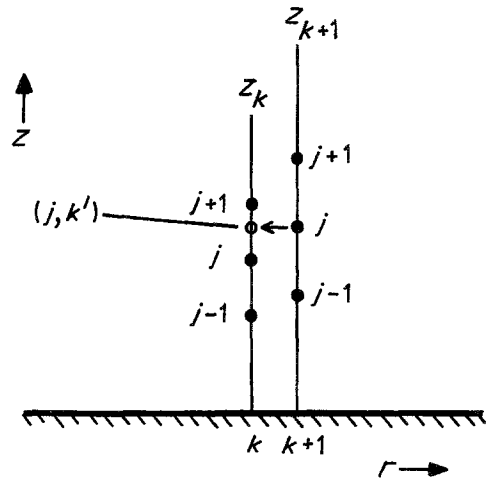

Fig. 5. The interpolation of the concentration at the point (j, k').

grid is required [17]. To obtain this, we use the spacing as set along z_{k+1} (i.e. Z_{k+1}/J) and find the concentration of A at corresponding points along z_k by interpolation as can be understood by reference to Fig. 5. Consider the concentrations at the points $(j - 1, k)$, (j, k) and $(j, k + 1)$ which are known and from which the concentration at the point $(j, k + 1)$ is to be calculated. In order to do this we need to know (see below) the concentration at the point (j, k') (which represents an interpolated point in the Cartesian space as defined by J 'boxes' along the line z_{k+1}).

If we consider the ratio of the length of adjacent grid lines

$$\{z_{k+1}/z_k\} = \{(k + 1)/k\}^{5/4} \tag{18}$$

we see that for small k, the grid is expanding very rapidly (for example $z_2 > 2z_1$). Thus for small k, Fig. 5 is incorrect in the sense that the point (j, k) does not necessarily lie between $(j, k + 1)$ and $(j + 1, k + 1)$. We therefore estimate (j, k') by the following means

(a) For j such that

$$\{j/J\}z_{k+1} > z_k \quad \text{then, } g_{j,k'} = 1 \tag{19}$$

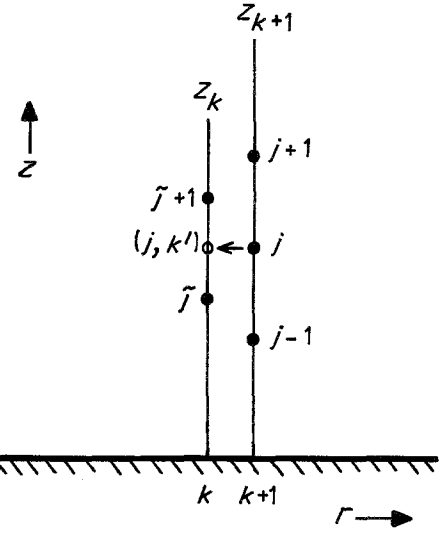

Fig. 6. Diagram illustrating the parameter $\tilde{j}$.

(b) For lower j, it is necessary to identify $\tilde{j}$ and $(\tilde{j} + 1)$ (as shown in Fig. 6) such that

$$\{(\tilde{j} + 1)/J\}z_k > \{j/J\}z_{k+1} > \{\tilde{j}/J\}z_k \quad (20)$$

so that Lagrangian two-point interpolation may be used to find the concentration at (j, k')

$$g_{j,k'} = g_{j,k} + \{g_{\tilde{j}+1,k} - g_{j,k}\}(J/z_k)\,p \quad (21)$$

where p is a weighting factor

$$p = (j/J)z_{k+1} - (\tilde{j}/J)z_k \quad (22)$$

The finite-difference representation of the derivatives in the convective-diffusion equations of interest in terms of the expanding grid notation is as in Equations 11–13 except that $g_{j,k}$ is replaced by $g_{j,k'}$ in Equation 11.

The implementation of the expanding grid theory requires us to specify v_r and v_z in a computationally compatible form. Firstly we choose to 'centre' the velocity terms on the point $(j, k + 1)$:

$$v_r(r, z) = v_r((k + 1)\Delta r, j\Delta z) \quad (23)$$

$$v_z(r, z) = v_z((k + 1)\Delta r, j\Delta z) \quad (24)$$

Secondly, since concentration changes are restricted to small values of η, we can use the following approximate equations in place of the full Equations, Equations 2 and 3, [11]

$$v_{r,\eta\to 0} = (2/9)\,(15M/2vr^3)\,\eta \quad (25)$$

$$v_{z,\eta\to 0} = (7/36)\,(40Mv/3r^5)\,\eta^2 \quad (26)$$

Substitution of the relevant equations into Equation 8 gives

$$\{g_{j,k+1} - g_{j,k'}\} + \lambda_{j,k+1}\{g_{j+1,k+1} - g_{j,k+1}\} = \varepsilon_{j,k+1}\{g_{j+1,k+1} - 2g_{j,k+1} + g_{j-1,k+1}\} \quad (27)$$

where

$$\lambda_{j,k+1} = \frac{v_z(j, k + 1)\Delta r}{v_r(j, k + 1)\Delta z} \quad (28)$$

$$\varepsilon_{j,k+1} = \frac{D\Delta r}{v_r(j, k + 1)\,(\Delta z)^2} \quad (29)$$

Rearrangement of Equation 27 gives us the general equation for the Backwards Implicit calculation:

$$g_{j,k'} = -\varepsilon_{j,k+1}\,g_{j-1,k+1} + \{2\varepsilon_{j,k+1} - \lambda_{j,k+1} + 1\}\,g_{j,k} - \{\varepsilon_{j,k+1} - \lambda_{j,k+1}\}\,g_{j+1,k+1} \quad (30)$$

Application of the boundary conditions to Equation 30 gives

(a) at the electrode surface, $g_{0,k} = 0$, so

$$g_{1,k'} = \{2\varepsilon_{1,k+1} - \lambda_{1,k+1} + 1\}\,g_{1,k} - \{\varepsilon_{1,k+1} - \lambda_{1,k+1}\}\,g_{2,k+1} \quad (31)$$

(b) at the edge of the diffusion layer, $g_{J,k} = 1$, so

$$g_{J-1,k'} = -\varepsilon_{J-1,k+1}\,g_{J-2,k+1} + \{2\varepsilon_{J-1,k+1} - \lambda_{J-1,k+1} + 1\}\,g_{J-1,k} - \{\varepsilon_{J-1,k-1} - \lambda_{J-1,k+1}\} \quad (32)$$

These $(J - 1) \times (J - 1)$ simultaneous equations may be expressed as a $(J - 1) \times (J - 1)$ matrix equation:

$$\{d\} = [T]\{u\} \quad (33)$$

i.e.

$$\begin{bmatrix} d_1 \\ d_2 \\ \cdot \\ \cdot \\ \cdot \\ d_j \\ \cdot \\ \cdot \\ \cdot \\ d_{J-2} \\ d_{J-1} \end{bmatrix} = \begin{bmatrix} b_1 & c_1 & 0 & & & & \\ a_2 & b_2 & c_2 & 0 & & & \\ & \ddots & \ddots & \ddots & \ddots & & \\ 0 & a_j & b_j & c_j & 0 & & \\ & & \ddots & \ddots & \ddots & \ddots & \\ & & & a_{J-2} & b_{J-2} & c_{J-2} & \\ & & & 0 & a_{J-1} & b_{J-1} & \end{bmatrix} \begin{bmatrix} u_1 \\ u_2 \\ \cdot \\ \cdot \\ \cdot \\ u_j \\ \cdot \\ \cdot \\ \cdot \\ u_{J-2} \\ u_{J-1} \end{bmatrix}$$

where

$$d_j = g_{j,k'} \qquad j = 1, 2, \ldots, (J - 2) \quad (34)$$

$$d_{J-1} = g_{J-1,k'} + \{\varepsilon_{J-1,k+1} - \lambda_{J-1,k+1}\} \quad (35)$$

$$u_j = g_{j,k+1} \qquad j = 1, 2, \ldots, (J - 1) \quad (36)$$

$$a_j = -\varepsilon_{j,k+1} \qquad j = 2, 3, \ldots, (J - 1) \quad (37)$$

$$b_j = (2\varepsilon_{j,k+1} - \lambda_{j,k+1} + 1) \quad j = 1, 2, \ldots, (J - 1) \quad (38)$$

$$c_j = -(\varepsilon_{j,k+1} - \lambda_{j,k+1}) \qquad j = 1, 2, \ldots, (J - 2) \quad (39)$$

The matrix $[T]$ is of tridiagonal form and this allows the use of the Thomas Algorithm [17, 26] to calculate $\{u\}_k$ from $\{d\}_k$. The boundary condition $g_{j,0} = 1$ $(j = 1, 2, \ldots, J)$ supplies the vector $\{d\}_0$ from which $\{u\}_0$ is calculated. However $\{d\}_{k+1}$ is readily determined from $\{u\}_k$ (Equations 34–36) so that $\{u\}_1$ may then be calculated from $\{d\}_1$, $\{u\}_2$ from $\{d\}_2$, and so on until $\{u\}_K$ is obtained. In this way all the values $g_{j,k}$ $(j = 1, 2, \ldots, (J - 1), k = 1, \ldots, K)$ can be evaluated. Notice that this is achieved without the need to specify a value for $g_{0,0}$. This feature makes the Backwards Implicit Method particularly appropriate for wall-jet problems – the fact that the diffusion layer is infinitesimally thin at $r = 0$ enables us to use $g_{j,0} = 1$ $(J = 1, 2, \ldots, J)$ as an initial boundary condition from which concentrations 'downstream' of $r = 0$ may be calculated.

The expression for the transport-limited current, I, at the electrode takes the form:

$$I = \int_0^R 2\pi rDF\left.\frac{\partial c}{\partial r}\right|_{z=0} \mathrm{d}r \quad (40)$$

where F is Faraday's constant. This is computed from the following equation

$$I = \sum_{k=1}^{K} 2\pi kDF[\mathrm{A}]_0\,\frac{g_{1,k}}{\Delta z}\,(\Delta r)^2 \quad (41)$$

4. The ECE mechanism

In this section the Expanding Grid Backwards Implicit Method is extended to include the coupled kinetics of the ECE mechanism. The mechanism is defined by the following kinetic scheme

$$\begin{aligned} &\text{E} \quad \text{A} + e^- \longrightarrow \text{B} \\ &\text{C} \quad \text{B} \xrightarrow{k_1} \text{C} \\ &\text{E} \quad \text{C} + e^- \longrightarrow \text{P} \end{aligned} \qquad \text{(II)}$$

The associated steady-state transport equations are

$$v_r \frac{\partial a}{\partial r} + v_z \frac{\partial a}{\partial z} = D \frac{\partial^2 a}{\partial z^2} \qquad (42)$$

$$v_r \frac{\partial b}{\partial r} + v_z \frac{\partial b}{\partial z} = D \frac{\partial^2 b}{\partial z^2} - k_1 b \qquad (43)$$

$$v_r \frac{\partial c}{\partial r} + v_z \frac{\partial c}{\partial z} = D \frac{\partial^2 c}{\partial z^2} + k_1 b \qquad (43)$$

where we have made the approximation that A, B and C have the same diffusion coefficient, D. We further assume that only A is present in bulk solution and normalise the concentrations of the three species relative to $[A]_0$: $g^A = [A]/[A]_0$, $g^B = [B]/[A]_0$ and $g^C = [C]/[A]_0$. The boundary conditions corresponding to transport-limited conditions are

$$\text{(a) } r = 0\text{: } g^A = 1, \quad g^B = g^C = 0 \qquad (45)$$

$$\text{(b) } z = 0\text{: } g^A = 0, \quad \partial g^B/\partial z = -\partial g^C/\partial z, \quad g^C = 0 \qquad (46)$$

$$\text{(c) } z \longrightarrow \infty \ (\eta = \eta^*)\text{: } g^A = 1, \quad g^B = g^C = 0 \qquad (47)$$

Applying the method used for the simple electron-transfer case we obtained three matrix equations, one for each of i = A, B and C such that:

$$\{d\}^i = [T]^i\{u\}^i \qquad (48)$$

We next work out the matrix elements for B and C; those of A are unchanged from the previous case. By substituting the relevant finite-difference equations into Equation 43 we obtain the following general Backwards Implicit equation for B

$$g^B_{j,k'} = -\varepsilon_{j,k+1} g^B_{j-1,k+1} + \{2\varepsilon_{j,k+1} - \lambda_{j,k+1} + 1 + K_{j,k+1}\} g^B_{j,k+1} - \{\varepsilon_{j,k+1} - \lambda_{j,k+1}\} g^B_{j+1,k+1} \qquad (49)$$

where $\lambda_{j,k+1}$ and $\varepsilon_{j,k+1}$ are as defined above and K is given by

$$K_{j,k+1} = \frac{k_1 \Delta r}{v_r(j, k+1)} \qquad (50)$$

Applying the boundary conditions (b) and (c) above we find that

$$g^B_{1,k+1} - g^B_{0,k+1} = -g^A_{1,k+1} \qquad (51)$$

and $g^B_{J,k} = 0$. Applying these constraints to Equation 49, we can then identify the required matrix elements for B

$$d_j = g^B_{j,k'} \qquad j = 2, 3, \ldots, (J-2) \qquad (52)$$

$$d_1 = g^B_{1,k'} + \varepsilon_{1,k+1} g^A_{1,k+1} \qquad (53)$$

$$u_j = g^B_{j,k+1} \qquad j = 1, 2, \ldots, (J-1) \qquad (54)$$

$$a_j = -\varepsilon_{j,k+1} \qquad j = 2, 3, \ldots, (J-1) \qquad (55)$$

$$b_j = (2\varepsilon_{j,k+1} - \lambda_{j,k+1} + 1 + K_{j,k+1}) \qquad j = 2, 3, \ldots, (J-1) \qquad (56)$$

$$b_1 = (\varepsilon_{1,k+1} - \lambda_{1,k+1} + 1 + K_{1,k+1}) \qquad (57)$$

$$c_j = -(\varepsilon_{j,k+1} - \lambda_{j,k+1}) \qquad j = 1, 2, \ldots, (J-2) \qquad (58)$$

Repeating the above procedure, we obtain the general Backwards Implicit equation for C

$$g^C_{j,k'} + K_{j,k+1} g^B_{2j,k+1} = -\varepsilon_{j,k+1} g^C_{j-1,k+1} + \{2\varepsilon_{j,k+1} - \lambda_{j,k+1} + 1\} g^C_{j,k+1} - \{\varepsilon_{j,k+1} - \lambda_{j,k+1}\} g^C_{j+1,k+1} \qquad (59)$$

Applying again the boundary conditions (b) and (c) we obtain $g^C_{0,k+1} = 0$ and $g^C_{J,k} = 0$ and can thus deduce the sought matrix elements

$$d_j = g^C_{j,k'} + K_{j,k+1} g^B_{j,k+1} \qquad j = 1, 2, \ldots, (J-1) \qquad (60)$$

$$u_j = g^C_{j,k+1} \qquad j = 1, 2, \ldots, (J-1) \qquad (61)$$

$$a_j = -\varepsilon_{j,k+1} \qquad j = 2, 3, \ldots, (J-1) \qquad (62)$$

$$b_j = (2\varepsilon_{j,k+1} - \lambda_{j,k+1} + 1) \qquad j = 1, 2, \ldots, (J-1) \qquad (63)$$

$$c_j = -(\varepsilon_{j,k+1} - \lambda_{j,k+1}) \qquad j = 1, 2, \ldots, (J-2) \qquad (64)$$

It can be seen that the matrix elements for B depend on $g^A_{j,k+1}$ and the matrix elements of C on $g^B_{j,k+1}$, so that the matrix equations for each k value must be solved in the order A then B then C before proceeding to the next value of k (i.e. $k + 1$).

The current is the sum of that due to the reduction of both A and C

$$I = \sum_{k=1}^{K} 2\pi k DF[A]_0 \frac{g^A_{1,k} + g^C_{1,k}}{\Delta z} (\Delta r)^2 \qquad (65)$$

5. The DISP1 mechanism

In this section the theory for the DISP1 reaction is established. The reaction mechanism is defined by the

following scheme

$$\begin{aligned} &\text{E} && \text{A} + e^- \longrightarrow \text{B} \\ &\text{C} && \text{B} \xrightarrow{k_1} \text{C} \\ &\text{DISP} && \text{B} + \text{C} \longrightarrow \text{A} + \text{P (fast)} \end{aligned} \qquad \text{(III)}$$

The appropriate steady-state transport equations are

$$v_r \frac{\partial a}{\partial r} + v_z \frac{\partial a}{\partial z} = D \frac{\partial^2 a}{\partial z^2} + k_1 b \qquad (66)$$

$$v_r \frac{\partial b}{\partial r} + v_z \frac{\partial b}{\partial z} = D \frac{\partial^2 b}{\partial z^2} - 2k_1 b \qquad (67)$$

and the boundary conditions for transport-limited conditions

$$\text{(a) } r = 0\text{: } g^{\text{A}} = 1, \quad g^{\text{B}} = 0 \qquad (68)$$

$$\text{(b) } z = 0\text{: } g^{\text{A}} = 0, \quad \partial g^{\text{B}}/\partial z = -\partial g^{\text{A}}/\partial z \qquad (69)$$

$$\text{(c) } z \longrightarrow \infty \ (\eta = \eta^*)\text{: } g^{\text{A}} = 1, \quad g^{\text{B}} = 0 \qquad (70)$$

Again we have $\{d\}^i = [T]^i\{u\}^i$ where i = A and B, and we need to work out the corresponding matrix elements.

The general Backwards Implicit equation for A is given by

$$g^{\text{A}}_{j,k'} + K_{j,k+1} g^{\text{B}}_{2j,k+1} = -\varepsilon_{j,k+1} g^{\text{A}}_{j-1,k+1} + \{2\varepsilon_{j,k+1} - \lambda_{j,k+1} + 1\} g^{\text{A}}_{j,k+1} - \{\varepsilon_{j,k+1} - \lambda_{j,k+1}\} g^{\text{A}}_{j+1,k+1} \qquad (71)$$

Applying the boundary conditions $g^{\text{A}}_{0,k+1} = 0$ and $g^{\text{A}}_{J,k+1} = 1$ we obtain the following matrix elements

$$d_j = g^{\text{A}}_{j,k'} + K_{j,k+1} g^{\text{B}}_{j,k+1} \qquad j = 1, 2, \ldots, (J-2) \qquad (72)$$

$$d_{J-1} = g^{\text{A}}_{J-1,k'} + K_{J-1,k+1} g^{\text{B}}_{J-1,k+1} + (\varepsilon_{J-1,k+1} - \lambda_{J-1,k+1}) \qquad (73)$$

$$u_j = g^{\text{A}}_{j,k+1} \qquad j = 1, 2, \ldots, (J-1) \qquad (74)$$

$$a_j = -\varepsilon_{j,k+1} \qquad j = 2, 3, \ldots, (J-1) \qquad (75)$$

$$b_j = (2\varepsilon_{j,k+1} - \lambda_{j,k+1} + 1) \quad j = 1, 2, \ldots, (J-1) \qquad (76)$$

$$c_j = -(\varepsilon_{j,k+1} - \lambda_{j,k+1}) \qquad j = 1, 2, \ldots, (J-2) \qquad (77)$$

In the case of B we have the general equation

$$g^{\text{B}}_{j,k'} = -\varepsilon_{j,k+1} g^{\text{B}}_{j-1,k+1} + \{2\varepsilon_{j,k+1} - \lambda_{j,k+1} + 2K_{j,k+1} + 1\} g^{\text{B}}_{j,k+1} - (\varepsilon_{j,k+1} - \lambda_{j,k+1}) g^{\text{B}}_{j+1,k+1} \qquad (78)$$

The boundary condition in Equation 51 again applies along with $g^{\text{B}}_{J,k+1} = 0$ and so the matrix elements are

$$d_j = g^{\text{B}}_{j,k'} \qquad j = 2, 3, \ldots, (J-2) \qquad (79)$$

$$d_1 = g^{\text{B}}_{1,k'} + \varepsilon_{1,k+1} g^{\text{A}}_{1,k+1} \qquad (80)$$

$$u_j = g^{\text{B}}_{j,k+1} \qquad j = 1, 2, \ldots, (J-1) \qquad (81)$$

$$a_j = -\varepsilon_{j,k+1} \qquad j = 2, 3, \ldots, (J-1) \qquad (82)$$

$$b_j = (2\varepsilon_{j,k+1} - \lambda_{j,k+1} + 1 + 2K_{j,k+1}) \qquad j = 2, 3, \ldots, (J-1) \qquad (83)$$

$$b_1 = (\varepsilon_{1,k+1} - \lambda_{1,k+1} + 1 + 2K_{1,k+1}) \qquad (84)$$

$$c_j = -(\varepsilon_{j,k+1} - \lambda_{j,k+1}) \quad j = 1, 2, \ldots, (J-2) \qquad (85)$$

As can be seen from Equations 72, 73 and 80, the matrix elements for A depend on $g^{\text{B}}_{j,k+1}$ and those for B depend on $g^{\text{A}}_{j,k+1}$. Thus in order to facilitate solution of the equations we employ an iterative method. Specifically, an initial value of $g^{\text{B}}_{j,k'}$ for $g^{\text{B}}_{j,k+1}$ is assumed in order to permit the calculation of a value for $g^{\text{A}}_{j,k+1}$. This value is then used to calculate a 'better' value of $g^{\text{B}}_{j,k+1}$, and the process repeated until there is no significant change in either $g^{\text{A}}_{j,k+1}$ or $g^{\text{B}}_{j,k+1}$ on further iteration. The final values are then used to start the iterative calculation on the next line 'downstream', i.e. z_{k+2}. The current for the DISP1 case is given by Equation 41.

6. Results and discussion

6.1. *Simple electron-transfer*

We consider first the results obtained for the case of simple electron-transfer computed as described above. The convergence was examined by varying J and K. A value of $J = 200$ and $K = 5000$ was sufficient to give convergence to three significant figures in the computed current. These values were used to obtain the data discussed below. Fig. 7 shows a plot indicating how convergence is achieved by increasing K at the fixed value $J = 200$.

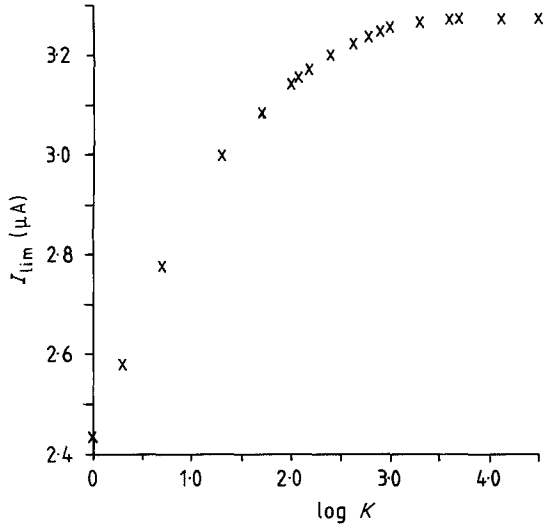

Fig. 7. The convergence of the transport-limited current for a simple electron transfer with log K, where K is the number of grid points on the radial direction. J was fixed at 200 in these calculations.

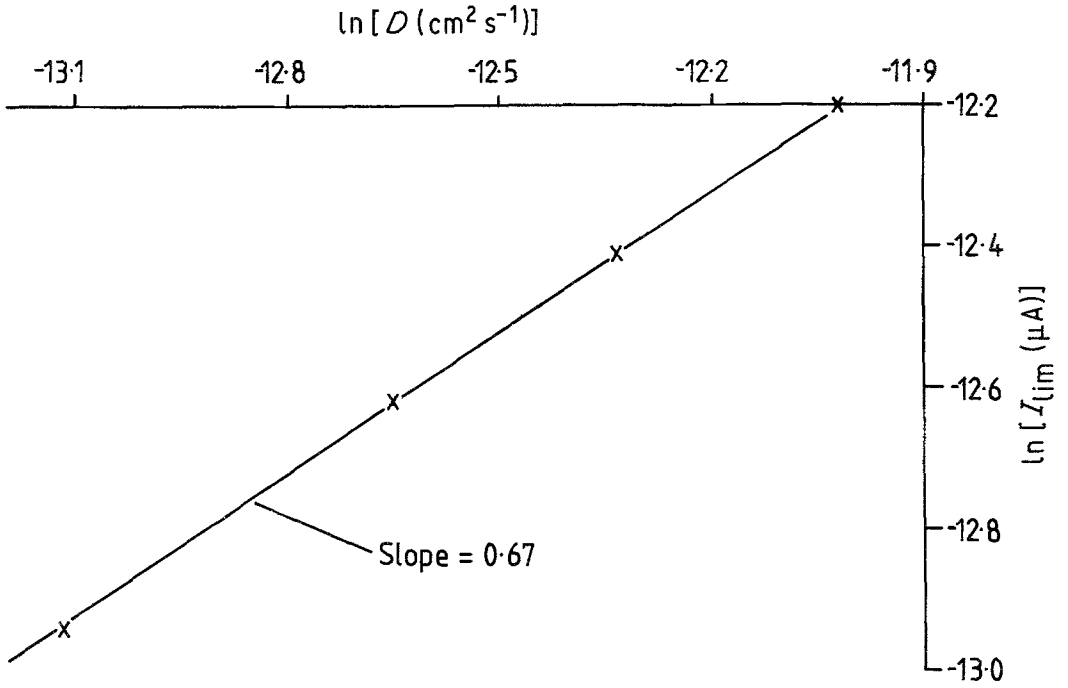

Fig. 8. The computed variation of $\ln(I)$ with $\ln(D)$ for a simple electron-transfer ($J = 200$, $K = 5000$, $V_f = 10^{-3}\,cm^3\,s^{-1}$). The line drawn has a slope of 2/3.

An analytical theory for the transport-limited current has been derived by Albery [11] from Equation 8, together with the approximations for v_r and v_z given in Equations 28 and 29

$$I = 1.59 k_c F D^{2/3} v^{-5/12} V_f^{3/4} a^{-1/2} R^{3/4} [A]_0 \quad (86)$$

in which it is assumed that the electrode reaction is a one-electron process. Albery's theory contains no different assumptions from the computational theory presented above and so the results obtained from our computations should be in good agreement with Equation 86. Plots of $\ln(I)$ with $\ln(D)$, $\ln(R)$ and $\ln(V_f)$ are shown in Figs 8–10 over the ranges $D = 2 \times 10^{-6}$ to $6 \times 10^{-6}\,cm^2\,s^{-1}$, $R = 0.1$ to 0.5 cm, and $V_f = 10^{-3}$ to $10^{-1}\,cm^3\,s^{-1}$. These plots were generated using the following parameters:

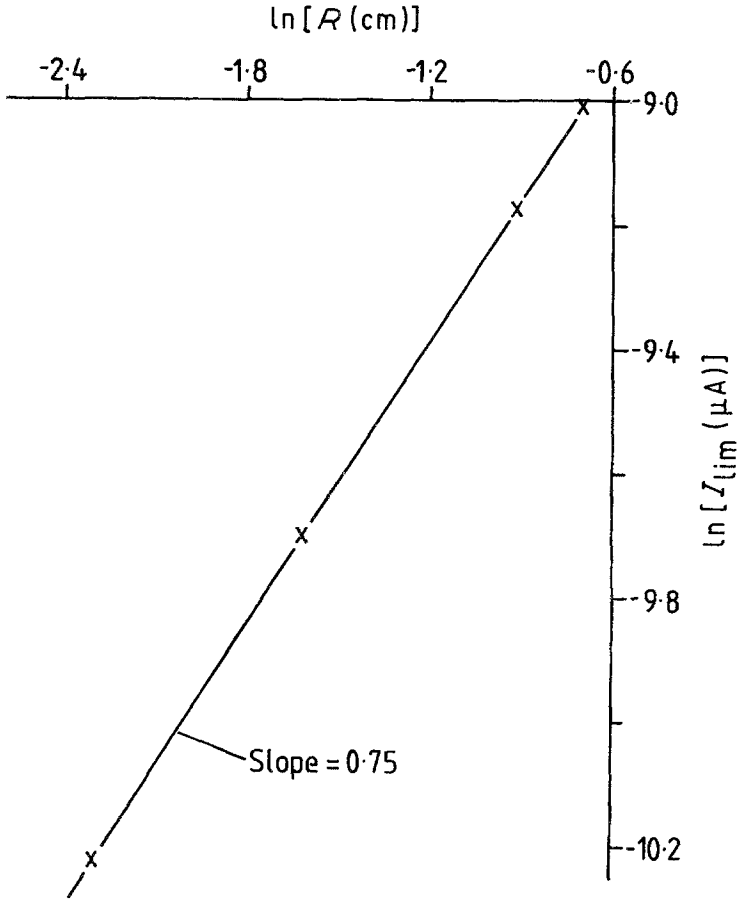

Fig. 9. The computed variation of $\ln(I)$ with $\ln(R)$ for a simple electron-transfer ($J = 200$, $K = 5000$, $V_f = 10^{-1}\,cm^3\,s^{-1}$). The line drawn has a slope of 3/4.

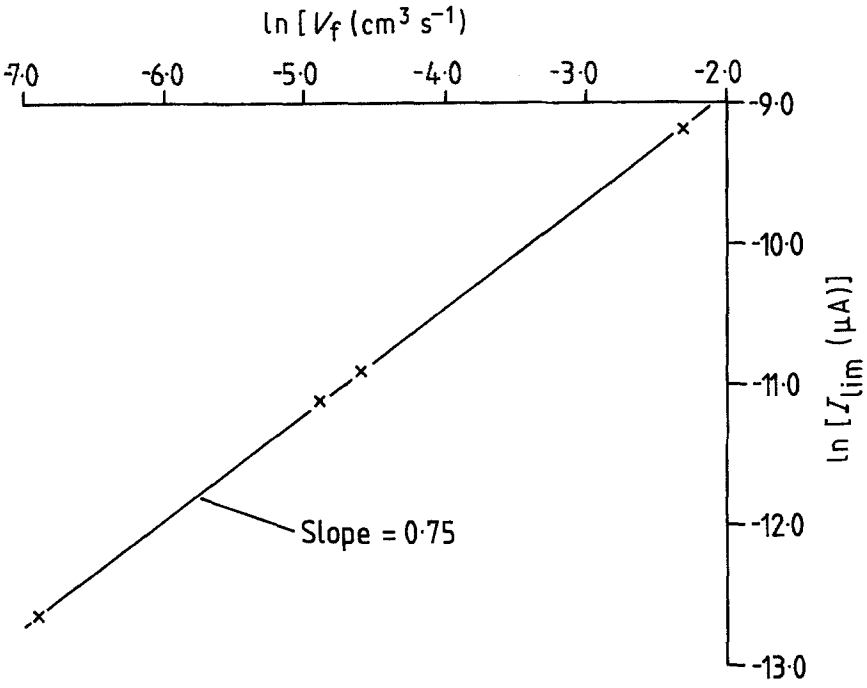

Fig. 10. The computed variation of ln (I) with ln (V_f) for a simple electron-transfer (J = 200, K = 5000). The line drawn has a slope of 3/4.

k_c = 0.9, v = 0.0089 cm^2 s^{-1} (H_2O), d = 3.2 × 10^{-6} cm^2 s^{-1}, R = 0.4025 cm and a = 0.0345 cm. It can be seen that the graphs have slopes of 0.67, 0.75 and 0.75 respectively, in excellent agreement with the analytical theory.

Different values of η^* were examined and the value of 0.4 found to be optimal. This was sufficiently large so that the concentration changes (of A) near to the electrode surface were confined to values of η appreciably smaller than 0.4 so as to validate the boundary condition $g^A_{J,k}$ = 1. At the same time, η^* = 0.4 is small enough to permit the use of the approximate equations for v_r and v_z, Equations 28 and 29.

The excellent agreement with analytical theory evident from Figs 8–10, together with the fact that the computations gave absolute values for the transport-limited current to within 1% of those predicted by Equation 86, over the ranges of D, R and V_f cited above, gives confidence in the general computational approach developed above. We thus encourage the general use of the Expanding Grid Backwards Implicit Method, in particular for those wall-jet problems where analytical theories are not available.

6.2. *ECE and DISP1 processes*

We consider next the results obtained for the ECE and DISP1 processes. In both cases the results are most conveniently displayed in terms of the effective

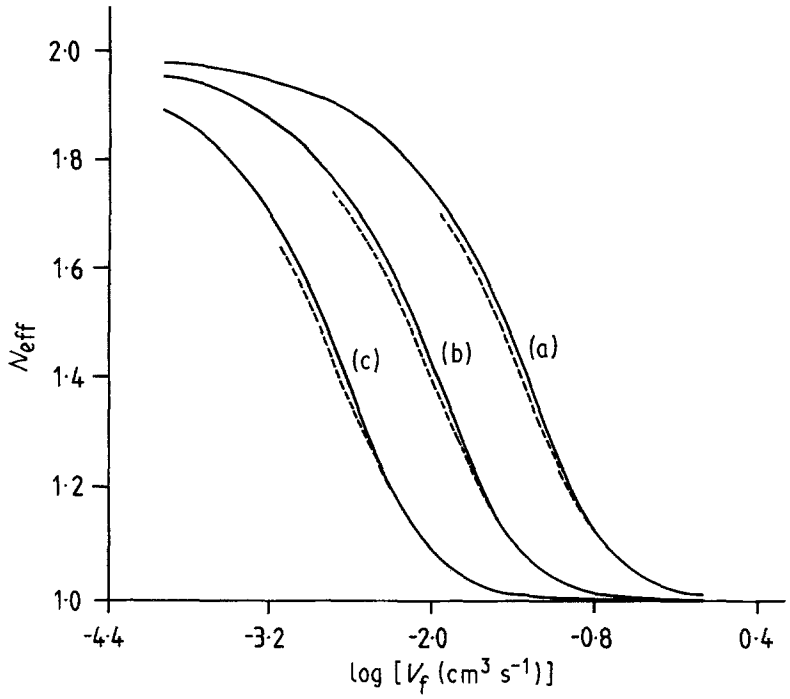

Fig. 11. The variation of N_{eff} with log (V_f) for the ECE (——) and DISP1 (– –) mechanisms for (a) k_1 = 1.0 s, (b) k_1 = 0.1 and (c) k_1 = 0.01 s^{-1}. The other parameters used in the computation are cited in the text.

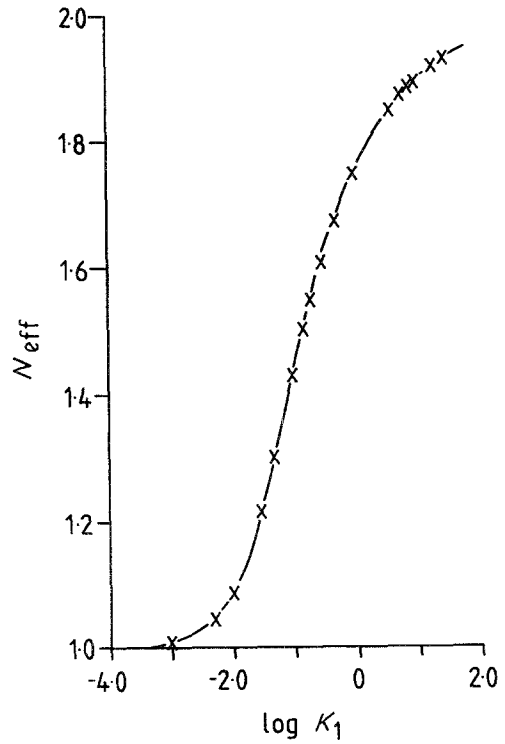

Fig. 12. A computed curve for the ECE mechansim showing how N_{eff} depends on the rate constant k_1 for the electrode of the geometry cited in the text, and a flow rate, $V_f = 10^{-2}\,cm^3\,s^{-1}$.

number of electrons transferred, N_{eff}, that is the ratio of the computed current to that calculated under identical conditions but with $k_1 = 0$. Calculations were performed using the same set of parameters as for the simple electron-transfer case above. In the case of the ECE reaction, convergence to three significant figures was readily achieved with $J = 200$ and $K = 5000$ for values of V_f between 5×10^{-5} and $1.0\,cm^3\,s^{-1}$ and values of k_1 between 10^{-4} and $30.0\,s^{-1}$. Typical results are shown in Fig. 11 and it can be seen that there is, as expected, a smooth transition between $N_{eff} = 2$ at low flow rates, and $N_{eff} = 1$ at fast flow rates. This reflects the competition between the loss of the intermediate B either from mass transport away from the electrode (high V_f) or through further reaction at the electrode (low V_f). Equivalently, Fig. 12 shows how N_{eff} depends on k_1 at a fixed flow rate for a WJE with the parameters defined above.

Satisfactory convergence in the DISP1 case was harder to achieve: $J = 500$ and $K = 6000$ only gave results to three significant figures for $k_1 < 5.0\,s^{-1}$ and for $V_f > 10^{-2}\,cm^3\,s^{-1}$. The results are shown in Fig. 11. The difference in the ease of convergence as compared to the ECE case can be attributed to the need to have $g^B_{j,k}$ as an accurate first approximation to $g^B_{j,k+1}$ when beginning the iteration to find $g^A_{j,k+1}$ and $g^B_{j,k+1}$. This dictates a finer grid than is necessary for the ECE calculation. Nevertheless, as can be seen from Fig. 11, satisfactory 'working curves' can be calculated covering almost the full range of the experimental variables.

6.3. *Mechanistic resolution*

Finally, it is interesting to compare the curves shown in Fig. 11 for the ECE and the DISP1 mechanism. It can be seen that there is a slight separation between the two working curves for a given rate constant and that, in principle, limiting current–flow rate data might allow the discrimination between these two closely related reaction mechanisms. However, for the electrode geometry used to generate Fig. 11, this would probably require experimental accuracies greater than those normally employed. Similarly

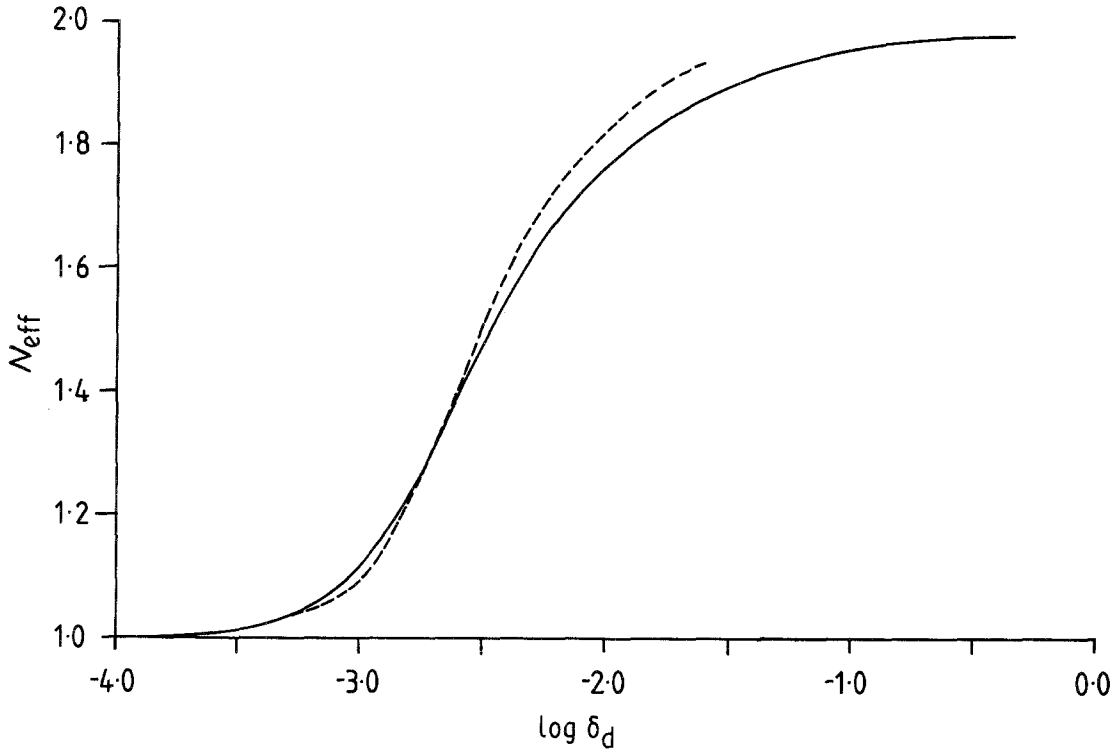

Fig. 13. A comparison of the theoretical curves of N_{eff} against diffusion-layer thickness for an ECE process at (a) the channel electrode (— —), and (b) the WJE (——).

pessimistic conclusions have been reached about the resolution of the ECE/DISP1 problem using steady-state rotating-disc electrode voltammetry [27, 28]. However, a more general and correct basis for a comparison between two different electrode types is to see how N_{eff} varies with the mean diffusion layer thickness, δ_d, of the electrode, rather than how it varies with V_f for some arbitrary electrode geometry

$$\delta_d = \frac{AFD[A]_0}{I} \qquad (87)$$

In this equation I is given by the appropriate transport-limited current equation for each electrode type and A is the area of the electrode.

6.4. *Comparison with channel electrode*

Fig. 13 shows a comparison between the wall-jet ECE response and that of a channel electrode (Fig. 14) under 'Levich conditions' [14, 15]. The latter has a diffusion layer thickness which increases as the cube root of the distance along its length. It is thus intermediate in behaviour between the uniformly accessible rotating-disc electrode and the wall-jet electrode (where δ_d varies as $r^{5/4}$). It can be seen that the non-uniformity of the WJE leads to a more gradual transition in N_{eff} between the extreme limits of $N_{eff} = 1$ and $N_{eff} = 2$ than is the case for the channel electrode. This may be understood as follows. It was explained above that N_{eff} reflects the competition between loss of intermediate (B) through transport into solution or through further heterogeneous charge-transfer at the electrode surface. At the upstream edge of a channel electrode, or at the centre of a WJE, the diffusion layer is very thin and this means that the concentration gradients here are very steep. This promotes the loss of intermediates from the electrode surface whereas further downstream, intermediates are more likely to undergo further electrode reaction as the diffusion layer is thicker and the concentration gradients are shallower, thus trapping intermediates. This will result in a gradual transition, in both types of electrode, from the transfer of one to two electrons as the flow rate is decreased. However, since the wall-jet is less uniformly accessible than the channel it is expected that this transition will be more gradual in that case.

Fig. 13 implies that the WJE is, in principle, intrinsically more sensitive than the channel electrode (which is itself superior to the rotating-disc electrode [15]) and is thus more likely to be able to resolve

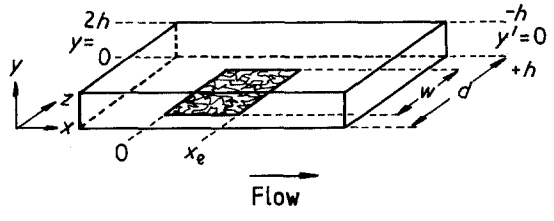

Fig. 14. A schematic drawing of a channel electrode. The electrode (shaded), of length x_e and width w, is embedded in the wall of a rectangular duct (cross-section $2hd$).

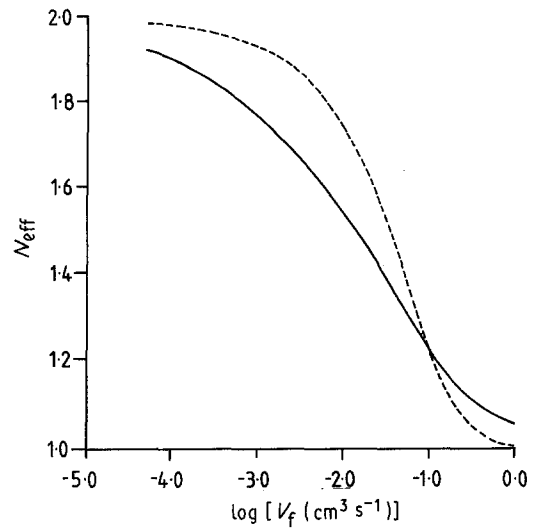

Fig. 15. 'Working curves' of N_{eff} against flow rate for the ECE process generated using typical dimensions (see text) for a channel electrode (——) and a WJE (— —).

closely similar types of electrode reaction mechanism. However, we have seen from Fig. 11 that for a typical practical wall-jet geometry ($R = 0.4$ cm), it is unlikely that the ECE and DISP1 processes could be resolved. Only with rather smaller electrode dimensions ($R < 0.1$ cm) would the resolution become feasible. In contrast we note that the ECE/DISP1 discrimination has been accomplished by N_{eff}–flow rate measurements at channel electrodes of convenient dimensions ($2h = 0.04$ cm, $w = 0.4$ cm, $d = 0.6$ cm, $x_e = 0.4$ cm; see Fig. 14) [14, 15]. The reason for this can be seen from Fig. 15 which shows, for an ECE process, how N_{eff} varies with flow rate for the WJE used in the calculations above and for the channel electrode cited. The latter is found to give a much gradual transition between the two limits and represents the superior of the two electrodes.

Clearly for maximum sensitivity WJEs need to be built as small as possible. However, a practical limitation on this is the requirement that the jet act as a point source in comparison with the electrode [1]. Thus the electrode always has to be appreciably larger in size than the jet, otherwise the hydrodynamics of the system are changed and the electrode becomes much more uniformly accessible [11]. No such restriction exists for channel electrodes which may thus prove to be more powerful than WJEs in the study of electrode reactions involving coupled homogeneous kinetics.

References

[1] M. B. Glauert, *J. Fluid. Mech.* **1** (1956) 625.
[2] H. Gunasingham, K. P. Ang and C. C. Ngo, *Anal. Chem.* **57** (1985) 505.
[3] J. Wang and B. A. Freiha, *ibid.* **57** (1985) 1776.
[4] H. Gunasingham, K. P. Ang, C. C. Ngo and P. C. Thiak, *J. Electroanal. Chem.* **198** (1986) 27.
[5] J. Wang, H. D. Dewald and B. Greene, *Anal. Chim. Acta* **146** (1983) 45.
[6] J. G. Douglas, *Anal. Chem.* **61** (1989) 922.
[7] H. Gunasingham, K. P. Ang and C. C. Ngo, *Analyst* **133** (1988) 1533.

[8] H. Gunasingham, B. T. Tay and K. P. Ang, *Anal. Chem.* **56** (1984) 2422.
[9] H. Gunasingham, *Anal. Chim. Acta.* **159** (1984) 2422.
[10] C. M. A. Brett and A. M. C. F. Oliveira Brett, *Comprehensive Chemical Kinetics* **26** (1986) 355.
[11] W. J. Albery and C. M. A. Brett, *J. Electroanal. Chem.* **148** (1983) 201.
[12] *Idem, ibid.* **148** (1983) 211.
[13] C. M. A. Brett and M. M. P. M. Neto, *J. Chem. Soc., Faraday Trans. I* **82** (1986) 1071.
[14] R. G. Compton and P. R. Unwin, *J. Electroanal. Chem.* **206** (1986) 1.
[15] P. R. Unwin and R. G. Compton, *Comprehensive Chemical Kinetics* **29** (1989) 173.
[16] J. Yamada and H. Matsuda, *J. Electroanal. Chem.* **44** (1973) 189.
[17] R. G. Compton, M. B. G. Pilkington and G. M. Stearn, *J. Chem. Soc., Faraday Trans. I* **84** (1988) 2155.
[18] J. L. Anderson and S. Moldoveanu, *J. Electroanal. Chem.* **179** (1984) 107.
[19] *Idem, ibid.* **179** (1984) 119.
[20] L. E. Fosdick and J. L. Anderson, *Anal. Chem.* **58** (1986) 2481.
[21] L. E. Fosdick, J. L. Anderson, T. A. Baginski and R. C. Jaeger, *ibid.* **58** (1986) 2750.
[22] T. Y. Ou, S. Moldoveanu and J. L. Anderson, *J. Electroanal. Chem.* **247** (1988) 1.
[23] R. G. Compton, G. M. Stearn, P. R. Unwin and A. J. Barwise, *J. Appl. Electrochem.* **18** (1988) 657.
[24] B. A. Coles, R. G. Compton and M. B. G. Pilkington, *J. Chem. Soc. Faraday Trans. I* **84** (1988) 4347.
[25] R. G. Compton and P. R. Unwin, *J. Electroanal. Chem.* **245** (1988) 303.
[26] L. Lapidus and G. Pinder, 'Numerical Solutions of Partial Differential Equations in Science and Engineering' (Wiley, New York, 1982).
[27] C. Amatore, M. Gareil and J. M. Saveant, *J. Electroanal. Chem.* **147** (1983) 1.
[28] C. Amatore and J. M. Saveant, *ibid.* **85** (1977) 27.